Research Article

Abul Arafat, Sabrin A. Samad, Jeremy J. Titman, Andrew L. Lewis, Emma R. Barney, and Ifty Ahmed*

Yttrium doped phosphate-based glasses: structural and degradation analyses

Abstract: This study investigates the role of yttrium in phosphate-based glasses in the system $45(P_2O_5)–25(CaO)–(30-x)(Na_2O)–x(Y_2O_3)$ $(0\leq x\leq 5)$ prepared via melt quenching and focuses on their structural characterisation and degradation properties. The structural analyses were performed using a combination of solid-state nuclear magnetic resonance (NMR), Fourier transform infrared spectroscopy (FTIR) and X-ray photoelectron spectroscopy (XPS). ^{31}P NMR analysis showed that depolymerisation of the phosphate network occurred which increased with Y_2O_3 content as metaphosphate units (Q^2) decreased with subsequent increase in pyrophosphate species (Q^1). The NMR results correlated well with structural changes observed via FTIR and XPS analyses. XRD analysis of crystallised glass samples revealed the presence of calcium pyrophosphate $(Ca_2P_2O_7)$ and sodium metaphosphate $(NaPO_3)$ phases for all the glass formulations explored. Yttrium-containing phases were found for the formulations containing 3 and 5 mol% Y_2O_3. Degradation analyses performed in Phosphate buffer saline (PBS) and Milli-Q water revealed significantly reduced rates with addition of Y_2O_3 content. This decrease was attributed to the formation of Y-O-P bonds where the octahedral structure of yttrium (YO_6) cross-linked phosphate chains, subsequently leading to an increase in chemical durability of the glasses. The ion release studies also showed good correlation with the degradation profiles.

Keywords: phosphate glass, Yttrium, ^{31}P NMR, FTIR, degradation and ion release profiles

*Corresponding Author: Ifty Ahmed: Faculty of Engineering, Advanced Materials Research Group, University of Nottingham, Nottingham NG7 2RD, United Kingdom;
Email: ifty.ahmed@nottingham.ac.uk

Abul Arafat, Sabrin A. Samad, Emma R. Barney: Faculty of Engineering, Advanced Materials Research Group, University of Nottingham, Nottingham NG7 2RD, United Kingdom

Jeremy J. Titman: School of Chemistry, University of Nottingham, University Park, Nottingham NG7 2RD, United Kingdom

1 Introduction

Biodegradable phosphate-based glasses (PBGs) have great potential in the field of biomaterials [1–5] due to their unique ability to totally resorb in aqueous media, which can be easily controlled via simple alteration of the glass formulations [6–8]. Other main advantages of phosphate glasses over other glasses (*i.e.* silicates) are their lower melting temperatures and ability to accommodate high concentrations of metal oxides [9–12]. However, ternary phosphate-based glass formulations (P_2O_5-Na_2O-CaO) are known to have relatively poor chemical durability which can limit their applications [6, 9]. To develop durable phosphate-based glasses, various transition metal oxides such as TiO_2 [11] and Fe_2O_3 [13] have been incorporated into phosphate glass formulations to enable control over their degradability.

Yttrium oxide containing glasses are an area of particular interest as Y_2O_3 has been shown to not only improve the glass durability and physical properties [14], but has also been demonstrated to be hugely beneficial for applications such as selective internal radiation therapy (SIRT) for treating liver cancers [15–17]. The yttrium aluminosilicate glass composition used for in situ radiation therapy (with formulation 17.1 mol% Y_2O_3, 18.9 mol% Al_2O_3, 64.0 mol% SiO_2) is known to be highly durable and non-resorbable [18, 19]. When this glass (in the form of solid microspheres) is activated by neutron bombardment they emit beta particles (from the Y^{90} isotope) which has a relatively short half-life of 64.2 h [20–22].

Due to shorter half-life, yttrium has led to some useful clinical applications to treat a range of diseases such as hepatocellular carcinoma [17], cushing's disease [23], arthritis [24] and used in a wide range of diagnostics and therapeutic applications such as PET [25], HP-MRI [26] and radiotherapy [27]. Borgonovo *et al.* found that yttrium stabilised zirconia can be used as a dental implant's mate-

Andrew L. Lewis: Biocompatibles UK Ltd, Lakeview, Riverside Way, Watchmoor Park, Camberley, GU15 3YL, United Kingdom

rial and they reported that incorporation of Y^{3+} into the crystal lattice of the smaller Zr^{4+} helped to produce stable cubic polymorphs of zirconia which subsequently beneficial for dental implants [28]. Neodymium doped yttrium aluminium garnets (Nd:YAG), have also been explored to treat cancer disease [29]. Furthermore, the role of yttrium oxide nanoparticles have been explored for nerve cells where Y_2O_3 nanoparticles acted as antioxidants that would be able to rescue cells from oxidative stress-induced cell death [30]. Toxicity levels of water-soluble compounds such as yttrium chlorides, yttrium nitrates are considered mildly toxic whilst its insoluble compounds such as yttrium oxides are non-toxic [31]. Dubois *et al.* studied the toxicity levels of yttrium chloride, nitrate and oxide in rats and reported that insoluble yttrium oxide (500 mg/kg) showed relatively non-toxic behaviour compared to soluble yttrium chloride (450 mg/kg) and yttrium nitrate (350 mg/kg) [32].

The structural effects of Y_2O_3 addition on silicate glasses have been reported in the literature. Singh *et al.* studied the structural changes of lithium borosilicate glasses with addition of 0 to 15 mol% Y_2O_3 and showed that Y_2O_3 acted as a network modifier as its concentration exceeded 5 mol% [33]. Simon *et al.* investigated iron-doped yttrium aluminosilicate glasses via XPS analysis and reported that Y_2O_3 played the role of network modifier oxide in the silicate glass network [34]. Fayad *et al.* also studied borosilicate glasses doped with Y_2O_3 and stated that Y_2O_3 preferred to act as a network modifier than network former especially at concentrations above 1 wt% [35].

The high durability of these silicate-based glass formulations mean that they remain in the body after treatment, potentially for years [14]. As such, developing bioresorbable glass microspheres (*i.e.* from phosphate glasses) containing yttrium with controlled and predictable degradation rates could be a major beneficial advantage over the existing silicate-based formulation.

The solubility of phosphate glasses is dependent on the glass composition [1]. The phosphate glass network is formed by linkages between PO_4 tetrahedral units which are described by Q^n notation where 'n' represents the number of bridging oxygens. Ultra-phosphate glasses (Q^3) represent PO_4 tetrahedra with three BO and one NBO, whereas metaphosphate glasses have Q^2 notation defined by tetrahedra with two BOs and two terminal oxygens [10]. Moreover, phosphate tetrahedra with one bridging oxygen (BO) and three NBOs are referred to as pyrophosphate (Q^1) species, whilst orthophosphate glasses (Q^0) represents four non-bridging oxygens (NBO) [6, 14]. In general, mainly Q^2 and Q^1 species have been observed for 45 mol% P_2O_5 containing glass formulations [36–38]. How-

ever, glasses with 50 mol% P_2O_5 theoretically consist of Q^2 units only whilst Q^3 species are also found in higher P_2O_5 containing glasses [36, 39]. Fu *et al.* conducted classical molecular dynamics simulations of the structure of yttrium doped phosphate-based glasses and reported that yttrium oxide acted as a network modifier due to depolymerisation of the phosphate network [40]. However, very limited physicochemical studies have been conducted before.

The crystallisation kinetics and ionic conductivity of yttrium phosphate glasses have been reported [41–44]. Petra *et al.* studied crystallisation kinetics of erbium-doped yttrium phosphate glasses for scintillation applications [45] by exploring the effect of particle sizes in both powder and bulk samples. They found that the activation energy decreased from 193 to 180 kJ/mol with increasing particle size. Martin *et al.* investigated the structural analysis of yttrium alumino-phosphate glasses using a combination of neutron diffraction, NMR and Vicker's hardness test [46]. From neutron diffraction and NMR experiments, they reported that yttrium acted as a network modifier where Y^{3+} cations preferentially bonded to the terminal oxygen atoms of PO_4 tetrahedra due to variation of coordination number with the substitution of Al_2O_3 by Y_2O_3. They also stated that the network connectivity of the glasses decreased with the increase of 0 to 26.3 mol% Y_2O_3 content which subsequently decreased the Vicker's hardness value from 792 to 410 kg mm^{-2}.

In this study, the effect of Y_2O_3 incorporation in ternary phosphate-based glass formulations fixed with 45 mol% P_2O_5 have been investigated. The structure of this glass system has been explored using solid-state magic angle spinning nuclear magnetic resonance (MAS-NMR), Fourier transform infrared (FTIR) and X-ray photoelectron (XPS) spectroscopies. The effect of adding Y_2O_3, on the ratio of bridging (BO) and non-bridging oxygens (NBO) has also been investigated. Moreover, chemical durability tests and pH analysis have been determined in phosphate-buffered saline (PBS) and Milli-Q water, along with the cation release data from these glasses.

2 Materials and methods

2.1 Glass preparation

Four different phosphate-based glass (PBG) formulations in the system $45P_2O_5$-$(30-x)Na_2O$-$25CaO$-xY_2O_3 were prepared using sodium dihydrogen phosphate (NaH_2PO_4), calcium hydrogen phosphate ($CaHPO_4$), yttrium oxide

Table 1: Glass codes, drying, melting and casting temperature used throughout the study

Glass Code	P_2O_5 content (mol%)	CaO content (mol%)	Na_2O content (mol%)	Y_2O_3 content (mol%)	Drying temp. / time (°C / hr)	Melting temp. / time (°C / hr)	Casting temp. / time (°C / hr)
Y0	45	25	30	—	350 / 0.5	1150 / 2	376 / 1
Y1	45	25	29	1	500 / 1	1300 / 2	387 / 1
Y3	45	25	27	3	500 / 1	1300 / 2	408 / 1
Y5	45	25	25	5	500 / 1	1300 / 2	434 / 1

(Y_2O_3) and phosphorous pentoxide (P_2O_5) as precursors (Sigma Aldrich, UK). The precursors were weighed, mixed and then transferred to a 10% Rh/Pt crucible (Birmingham Metal Company, UK), which was then placed in a furnace at 350°C for half an hour or 500°C for an hour depending on the glass compositions. The precursor mixtures were then transferred to another furnace and melted at 1150°C for 2 hours for the yttrium free glass and 1300°C for the yttrium-containing glasses, as highlighted in Table 1. The resultant molten glass was then poured onto a steel plate for quenching and left to cool to room temperature.

Samples of the glass formulations produced were then ground into powder utilising a mortar and pestle for further analyses. Having obtained their T_g, the glasses were cast into a graphite mould (9 mm diameter) which had been preheated to 10°C above T_g for each glass formulation. The mould was held at the respective casting temperature (see Table 1) for an hour and then cooled to room temperature. The rods obtained were cut into discs of approximately 5 mm thickness using a Testbourne diamond saw using Industrial Methylated Spirit (IMS) as a lubricant, for further analysis.

2.2 EDX analysis

To confirm the formulations produced, samples of each glass formulation were cast into epoxy resin followed by polishing with SiC paper and diamond cloth, using industrial methylated spirit (IMS) as an eluent. The samples were then dried before being carbon coated. EDX analysis was performed using an Oxford Instruments INCA EDX system with a Si–Li crystal detector. The EDX spectrometer was connected to an XL30 scanning electron microscope (FEI Company, USA) which was operated in secondary electron imaging mode, with an accelerating voltage of 15 kV, working distance of 10 mm and system resolution of 60 eV. Gallium phosphide (for P), jadeite (for Na), wollastonite (for Ca) and yttrium (for Y) were used as standard refer-

ences. Analysis was performed on five different areas of each glass sample.

2.3 Powder X-ray diffraction analysis

X-ray diffraction (XRD) analysis was used to explore the amorphous nature of each glass formulation. The data was collected on a Bruker AXS–D8 Advance powder diffractometer (BRUKER AXS, Germany) in flat plate geometry using Ni-filtered Cu-Kα radiation (λ = 0.15418 nm), operated at 40 kV and 35 mA where the angular range 2θ for each scan was from 10° to 70°. The step time was maintained 5 s with a step size of 0.1°. Phases were identified using the EVA software (DIFFRACplus suite, Bruker-AXS) and the International Centre for Diffraction Data (ICDD) database (2005).

Furthermore, milled glass powder was heat-treated at approximately 10°C above the crystallisation temperature (T_c) for 2 h in order to investigate the crystal phases of each glass formulation. Crystal phases were analysed using XRD analysis.

2.4 ³¹P NMR analysis

^{31}P NMR spectra were recorded at room temperature on a Varian Chemagnetics Infinityplus spectrometer operating at a Larmor frequency of 121.468 MHz using a 4 mm MAS probe spinning at 12 kHz. The ^{31}P $\pi/2$ pulse duration was 3.7 µs, the spectral width was 100 kHz and the acquisition time was 10.24 ms. Chemical shifts are quoted relative to 85% H_3PO_4 using $Na_4P_2O_7 \cdot 10H_2O$ as an external secondary reference. Prior to acquiring ^{31}P spectra the spin-lattice relaxation time T_1 was determined for each sample by saturation recovery. Saturation was achieved by 100 ^{31}P $\pi/2$ pulses spaced by delays of 5 ms with recovery delays of up to 1000 s. Quantitative ^{31}P NMR spectra required relaxation delays (5 T_1) of between 250 s and 600 s depending on the sample. The resulting spectra were deconvoluted

into a set of Gaussian lineshapes which were integrated in order to quantify the proportions of the different Q environments in the sample. MAS sidebands were included in the analysis.

2.5 FTIR analysis

Infrared spectroscopy of the glass particles was also performed using a Brüker Tensor 27 spectrometer (Brüker Optics, Germany) which was operated in absorbance mode. Spectra were measured in the region of 400 to 4000 cm^{-1} utilising a Standard Pike ATR cell (Pike Technologies, Inc., UK). OPUS software version 5.5 was used for the analysis.

2.6 XPS Analysis

XPS was performed using a VG Scientific ESCA Lab Mk2 electron spectrometer with a monochromatic Al KaX-ray source (1,486.6 eV) operated at 15 mA and 10 kV anode potential. For the XPS measurement, polished glass specimens were mounted onto a sample holder and readings were taken from three different areas. The shift of the binding energy due to surface charging effect was calibrated by referencing the measured binding energy of C 1s to 284.8 eV. For high-resolution spectra, 20 scans were taken using pass energy of 20 eV. CASA-XPS software was used for data processing and curve fitting of XPS spectra. These spectra were deconvoluted by using a best fit programme with Gaussian distributions.

2.7 Degradation analysis

To examine the differences in degradation profiles from the formulations produced, glass discs (9 mm diameter and 5 mm thickness) were placed in 30 ml Phosphate Buffer Saline (PBS) and Milli-Q-water with pH 7.5 and 7.4 respectively, at 37°C, in accordance with the degradation standard test conditions: ISO 10993-13:2010. The mass of each glass disc was obtained and their surface area was

measured using Mitutoyo Digimatic vernier callipers. After measuring the dimensions of each glass disc, they were then placed into vials and transferred to a 37°C oven. At various time points (1, 2, 3, 7, 14, 21 and 28 days), excess moisture was removed from the glass discs by blotting the samples dry with tissue. The mass and dimensions of the glass discs were recorded at each time point and then placed back into fresh media. The rate of mass loss (%) was calculated according to the following equation:

$$\text{Mass Loss (\%)} = \frac{M_0 - M_t}{M_0} \times 100 \qquad (1)$$

Where M_0 is the initial mass of the disc (g) and M_t is the mass at each time point. The pH of PBS and Milli-Q-water solutions were also determined. At each time point, three replicates of each sample were measured.

2.8 Ion release study

In order to determine the quantities of cations released, a Dionex ICS-1100 ion chromatography system (Dionex, UK) was used. A 20 mM MSA (Methanesulfonic acid, BDH, UK) solution was used as the eluent. The solution obtained at each time point from the degradation analysis in Milli-Q-water were analysed for sodium and calcium ion release. In this method, cations were eluted using a 2×250 mm IonPac1 CS12A separator column. The ICS-1100 performs isocratic ion chromatography (IC) separations using suppressed conductivity detection. Data analysis was conducted using Chromeleon7 software package. Dionex six cation-II standard (Li^+, Na^+, NH_4^+, K^+, Mg^{2+} and Ca^{2+} pH 3.0 ± 0.30, Thermo Scientific, UK) was used to produce calibration standards of 100, 50, 25, 10 and 1 ppm.

3 Results

3.1 EDX analysis

EDX analysis was performed to confirm the final glass compositions investigated (see Table 2). The differences

Table 2: Expected and actual chemical compositions from EDX analysis of the four glass formulations investigated in this study

| Sample	P_2O_5 (Expected / Actual value) (mol%)	CaO (Expected / Actual value) (mol%)	Na_2O (Expected / Actual value) (mol%)	Y_2O_3 (Expected / Actual value) (mol%)
Y0	45 / 44.1 ± 1.5	25 / 25.7 ± 1.3	30 / 30.2 ± 1.7	0 / 0
Y1	45 / 43.7 ± 1.2	25 / 26.7 ± 1.5	29 / 28.8 ± 1.4	1 / 0.8 ± 0.5
Y3	45 / 45.8 ± 1.8	25 / 25.7 ± 1.4	27 / 26.1 ± 1.3	3 / 2.4 ± 1.1
Y5	45 / 43.9 ± 1.8	25 / 26.1 ± 1.7	25 / 26 ± 1.9	5 / 4 ± 1.5

Table 3: ^{31}P NMR peak positions, relative proportions of Q^1 and Q^2 species and the calculated number of bridging oxygens (BOs) and non-bridging oxygens (NBOs) in the various glass formulations

Glass code	v(Q^1) /ppm	v(Q^2) /ppm	Intensity −8 ppm/ % (Q^1)	Intensity −22 ppm/ % (Q^2)	BO	NBO	BO/NBO	Phosphate chain length, L
Y0	−5.49	−21.74	22.78	77.22	1.77	2.23	0.79	8.69
Y1	−5.94	−21.57	27.11	72.89	1.73	2.27	0.76	7.41
Y3	−7.19	−21.82	33.90	66.10	1.66	2.34	0.71	5.88
Y5	−8.13	−21.92	41.15	58.85	1.59	2.41	0.66	4.88

between the expected values and actual values obtained were all within 0-2 mol%.

3.2 XRD analysis

The XRD profiles of the glass compositions are presented in Figure 1. A single broad halo peak was observed between 20° to 40° diffraction angle for each glass formulation investigated. Absence of any sharp crystalline peaks suggested that all the glasses produced were amorphous.
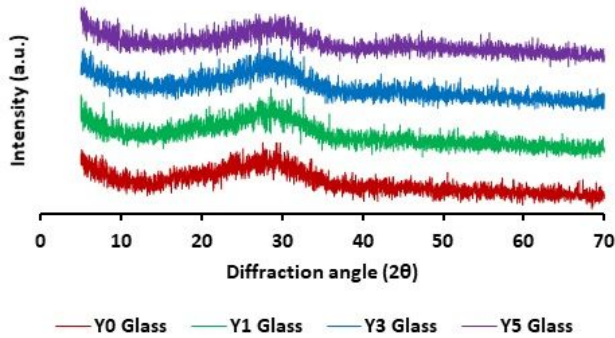
Figure 1: X-ray diffraction patterns for glasses in the system $45P_2O_5 - 25CaO - (30-x)Na_2O - xY_2O_3$ (where x = 0, 1, 3 and 5)

3.3 ^{31}P NMR analysis

^{31}P NMR analysis was performed to explore the structural connectivity of the phosphate network. Figure 2 shows the ^{31}P NMR spectra of the glass formulations investigated where each spectrum was fitted using Gaussian peaks centred at approximately −8 and −22 ppm and ascribed to Q^1 and Q^2 species respectively [47, 48]. The NMR spectra showed that the peaks associated with Q^1 and Q^2 species shifted from −5.49 to −8.13 ppm and from −21.74 to −21.92 ppm respectively with incorporation of Y_2O_3 (see Figure 2). The peak positions, relative proportions of Q^1 and Q^2

species and the ratio of bridging oxygens (BO) to non-bridging oxygens (NBO) for the individual glasses have been presented in Table 3. Significant variations in the relative intensity of Q species was observed between Y0 and Y5 glasses. For example, the relative intensity of Q^1 species increased from 22 to 41% whilst the intensity of Q^2 species decreased from 77 to 58% with increasing Y_2O_3 content (see Table 3). Furthermore, the average P$\cdots$P coordination number (N_{pp}) and average phosphate chain length (L) can be determined from the NMR Q-species [7, 49]. In addition, the N_{PP} is equal to the average number of bridging oxygen (N_{BO}) [50]. The N_{BO} and L are calculated using equations 2 and 3 and the results are presented in Table 3.

$$N_{BO} = f_Q^1 + 2f_Q^2 \tag{2}$$

$$L = \frac{-2}{N_{BO} - 2} \tag{3}$$

Where f_Q^n refers to the fraction of the Q^n group.
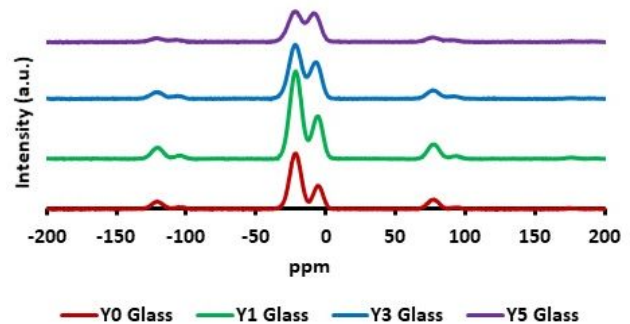
Figure 2: ^{31}P NMR spectra for glasses in the system $45P_2O_5 - 25CaO - (30-x)Na_2O - xY_2O_3$ (where x = 0, 1, 3 and 5)

The ratios of bridging oxygen (BO) to non-bridging oxygen (NBO) and phosphate chain length were seen to decrease from 0.79 to 0.66 and 8.69 to 4.88 respectively with the inclusion of Y_2O_3 content (0 to 5 mol%) as shown in Table 3.

Table 4: Theoretical calculation of Q species, BO to NBO ratio and chain length for different glass formulations

Sample	O/P	Q^1 species (%)	Q^2 species (%)	BO	NBO	BO/NBO	Phosphate chain length, n
Y0 glass	3.11	22	78	1.78	2.22	0.80	9
Y1 glass	3.13	26	74	1.74	2.26	0.77	7.49
Y3 glass	3.17	34	66	1.66	2.34	0.71	5.62
Y5 glass	3.22	44	56	1.56	2.44	0.64	4.50

3.4 Theoretical calculation of Q species, BO to NBO ratio and phosphate chain length

The expected percentage of Q species and BO to NBO ratio from each glass composition can be determined on the basis of oxygen to phosphorous ratio (O/P). As seen from Table 4, it was observed that the O/P ratios were in between metaphosphate (O/P=3, designated as Q^2) and pyrophosphate (O/P=3.5, termed as Q^1) regions for the glass formulations explored. According to glass composition region, the fraction of Q^2 can be calculated by following theoretical equation [51]:

$$f\left(Q^2\right) = \frac{3.5 - \left(\frac{O}{P}\right)}{0.5} \quad (4)$$

$$f\left(Q^1\right) = 100 - f(Q^2) \quad (5)$$

In addition, the number of BO in phosphate tetrahedral units can be evaluated by O/P ratio [50] and calculated using the equation 6 below:

$$N_{BO} = 8 - 2 \times (O/P) \quad (6)$$

Furthermore, the theoretical chain length (n) for 45 mol% phosphate based glasses can be determined using the following equation [52]:

$$n = \frac{2}{\left(\frac{M_{Na} + 2M_{Ca} + 3M_Y}{P}\right) - 1} \quad (7)$$

Where, M and P are the mole fraction of the cation and phosphorous respectively.

As seen in Table 4, the theoretical estimation of Q^1 species increased from 22 to 44%, whilst the Q^2 species decreased from 78 to 56% with increasing Y_2O_3 content into the glass system. Additionally, the BO to NBO ratio and phosphate chain length decreased from 0.80 to 0.64 and 9 to 4.50 respectively with the incorporation of 0 to 5 mol% Y_2O_3 as represented in Table 4. Overall, the theoretical percentage of Q species, BO to NBO ratio and chain length correlated well with the experimental NMR results.

3.5 FTIR analysis

FTIR analysis was also performed to explore any structural changes within the glasses produced. The spectra of each glass composition are presented in Figure 3. The absorption bands were assigned according to previous FTIR studies on phosphate based glasses [53–58]. The five main bands observed were at 703 cm^{-1}, 887 cm^{-1}, 970 cm^{-1}, 1095 cm^{-1} and 1265 cm^{-1} and their peaks assignments are provided in Table 5. The band at 703 cm^{-1} shifted to a higher wavenumber and intensity as Y_2O_3 was added into the glass system as presented in Figure 3. A similar change was also observed for the band at 970 cm^{-1} and 1095 cm^{-1}. The band at 887 cm^{-1} shifted to higher wavenumber (894 cm^{-1}) for 1 mol% Y_2O_3 and then decreased with the incorporation of 3 and 5 mol% Y_2O_3 into the glass system. The band at ~1265 cm^{-1} was noticed to shift to lower wavenum-

Table 5: FTIR band positions and assignments for different glass compositions

Wavenumbers (cm^{-1})	Assignments	Reference
703–719	Symmetric stretching vibrations of pyrophosphate groups (Q^1)	[107]
887–893	v_{as} (P-O-P), asymmetric stretching of the bridging oxygen atoms bonded to a phosphorus atom in a Q^2 phosphate tetrahedron.	[73]
970–976	v_s $(PO_3)^{2-}$, symmetric stretching modes of the chain terminating Q^1 groups.	[108]
1095–1113	v_{as} $(PO_3)^{2-}$, asymmetric stretching modes of the chain terminating Q^1 groups.	[109]
1245–1265	v_{as} $(PO_2)^-$, asymmetric stretching mode of the two non-bridging oxygens bonded to a phosphorous atom in Q^2 species.	[110]

bers with increased intensity with inclusion of Y_2O_3 content at the expense of Na_2O. The band near 2350 cm^{-1} indicates the presence of CO_2 [59].
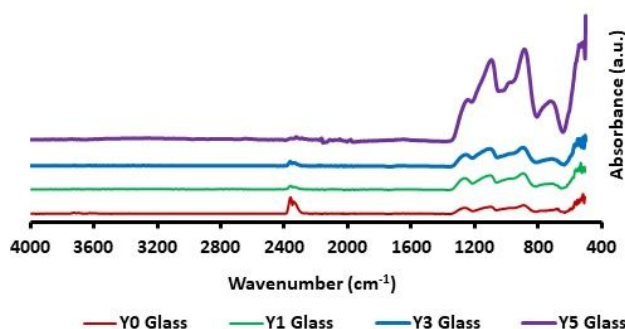

Figure 3: FTIR spectra for glasses in the system $45P_2O_5-25CaO-(30-x)Na_2O-xY_2O_3$ (where x = 0, 1, 3 and 5)

3.6 XRD profiles of Heat-treated glass formulations

XRD analysis of heat-treated glass compositions was performed to identify the crystal phases at crystallisation temperature. XRD patterns of heat-treated glasses are presented in Figure 4 and the crystalline phases were identified from XRD analysis (see Table 6). Y0 and Y1 glasses revealed peaks corresponding to calcium pyrophosphate ($Ca_2P_2O_7$), sodium metaphosphate ($NaPO_3$) and calcium sodium metaphosphate [$Na_4Ca(PO_3)_6$] phases. With further incorporation of 3 and 5 mol% yttrium oxide, sodium yttrium pyrophosphate ($NaYP_2O_7$) and sodium yttrium oxide ($NaYO_2$) phases were observed in place of the calcium sodium metaphosphate peak.
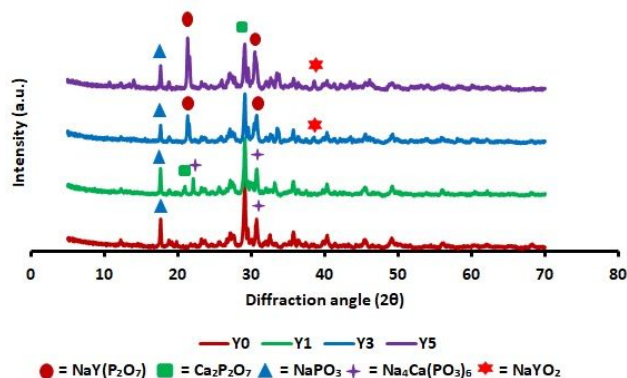

Figure 4: XRD patterns of the glass formulations heat-treated at their respective crystallisation temperatures

Table 6: Phases identified for different glass formulations using XRD and crystallographic software

Sample	Phase identified
Y0	$NaPO_3$, $Ca_2P_2O_7$, $Na_4Ca(PO_3)_6$
Y1	$NaPO_3$, $Ca_2P_2O_7$, $Na_4Ca(PO_3)_6$,
Y3	$NaPO_3$, $Ca_2P_2O_7$, $NaY(P_2O_7)$, $NaYO_2$
Y5	$NaPO_3$, $Ca_2P_2O_7$, $NaY(P_2O_7)$, $NaYO_2$

3.7 XPS analysis

XPS analysis was performed to provide information on the signature binding energy of the peaks from their different elements (as presented in Figure 5). The main signals in the spectrum were assigned to the glass constituents (P, O, Y, Na, Ca). Carbon content was also observed in the scan most likely from the ambient exposure of the samples before analysis. High-resolution O 1s spectra for the four glass compositions explored are depicted in Figure 6. The peaks from x = 0 to 5 were deconvoluted into two components each and the highest binding energy peak was referred to the bridging oxygen (BO) whilst the lowest binding energy peak was associated with non-bridging oxygen (NBO). The BO and NBO binding energy increased by 1.5 eV and 1.7 eV respectively with inclusion of Y_2O_3 into these glasses. The spectra obtained revealed that the BO/NBO ratio values decreased from 0.73 to 0.65 with incorporation

Table 7: BO/NBO ratios of different glass formulations from high resolution O 1s spectra

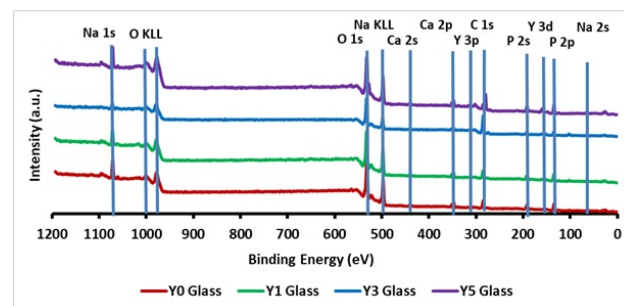| Sample Code	BO, Binding energy (eV)	NBO, Binding energy (eV)	BO/NBO (measured)-XPS
P45Y0	533.3	531.7	0.73
P45Y1	533.3	531.9	0.70
P45Y3	533.5	531.9	0.67
P45Y5	534.8	533.4	0.65

Figure 5: XPS survey scan for glasses in the system $45P_2O_5-25CaO-(30-x)Na_2O-xY_2O_3$ (where x = 0, 1, 3 and 5)
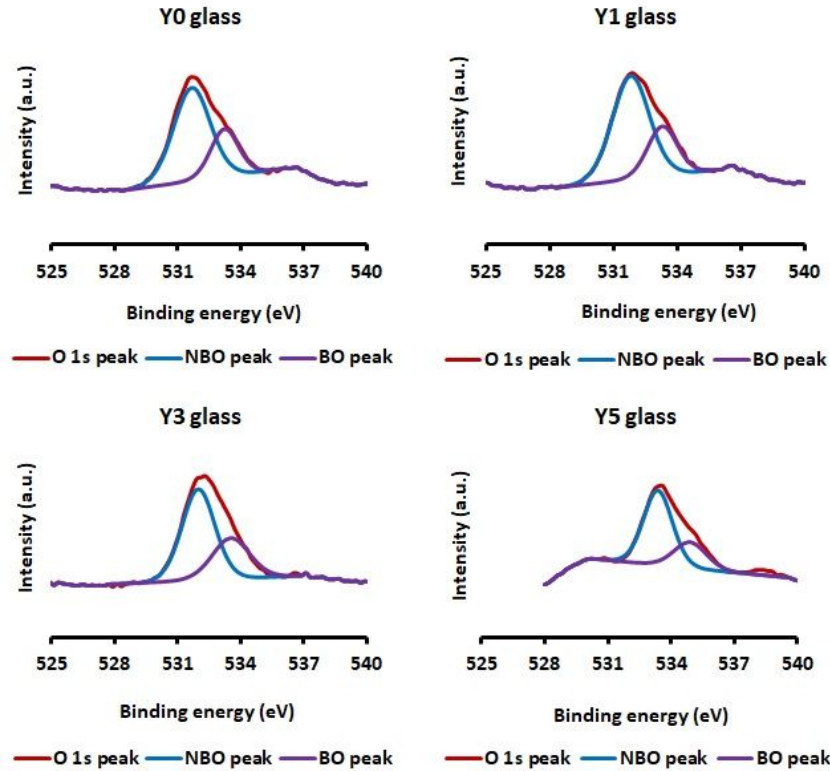
Figure 6: High resolution scans of the O 1s peak for glasses in the system $45P_2O_5-25CaO-(30-x)Na_2O-xY_2O_3$ (where x = 0, 1, 3 and 5)

of 0 to 5 mol% Y_2O_3 in the glass system as represented in Table 7.

3.8 Degradation and pH analysis

Degradation tests of the yttrium phosphate glass formulations (cut into discs) were carried out in phosphate buffered saline (PBS) solution and ultra-pure water (Milli-Q-water) at $37°C$ over 28 days (see Figure 7a and 7b respectively). All glass formulations followed an approximate linear profile of mass loss against degradation time in both PBS and Milli-Q water media. At the end of these degradation experiments, the percentage mass loss decreased gradually from 34.8% to 5.4% (in PBS) and 22.5% to 1.2% (in Milli-Q water) as Y_2O_3 content increased from 0 to 5
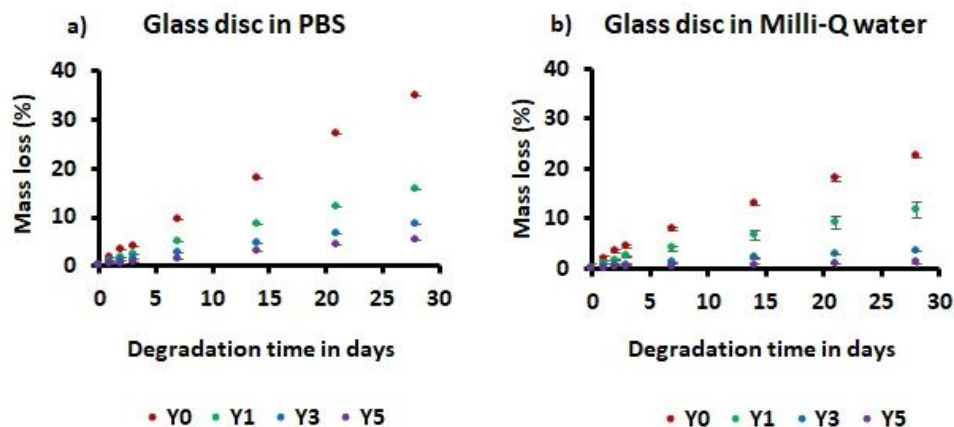

Figure 7: Dissolution study for the $45P_2O_5-(30-x) Na_2O-25CaO-xY_2O_3$ (where x = 0, 1, 3 and 5) glass system conducted in (a) PBS and (b) Milli-Q water at $37°C$
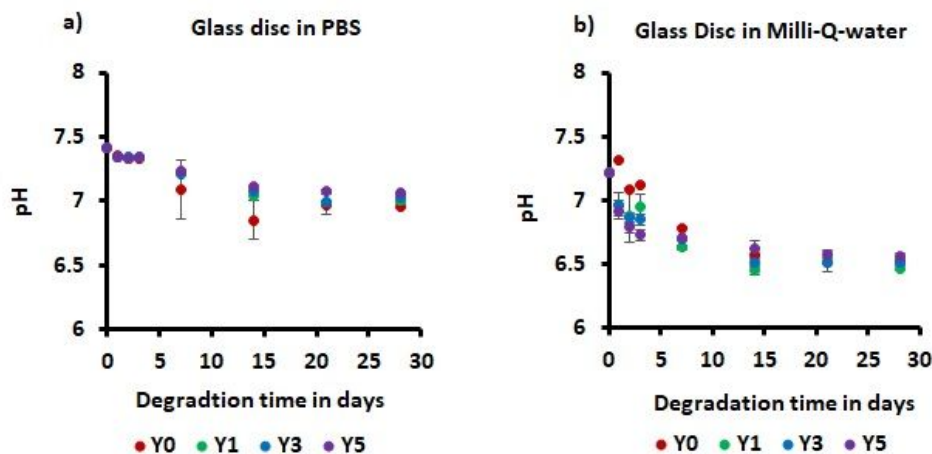
Figure 8: Change in pH of the degradation media as a function of time (day) of the produced glass disc in a) PBS and b) Milli-Q water up to 28 days. (Error bars represent ±SD)

mol% (see Figure 7). The rates of mass loss for all glass compositions in PBS were 30-70% faster than those degrading in Milli-Q water.

Figure 8 shows the change in pH of degradation media for the glass discs immersed in PBS and ultra-pure water (Milli-Q-water). From Figure 8a, little change in pH value (7.4 to 7.0) was observed in PBS up to 28 days for all glass formulations. However, the pH values of the control glass sample (Y0) in Milli-Q water changed from 7.2 to 6.51 by day 28. The other glass formulations also followed very similar profiles, respectively (see Figure 8a and 8b).

3.9 Ion release profiles

Profiles of cumulative Na^+ and Ca^{2+} ion release (in ppm) from glass disc were investigated as a function of time (day) and are presented in Figures 9(a) and 9(b) respectively. It was observed that the cumulative Na^+ and Ca^{2+} ion release for all the glass formulations followed a linear relationship over the 28 period of degradation study. For the Y0 glass formulation, the highest Na^+ and Ca^{2+} ion release was seen to reach 838 ppm and 507 ppm respectively at day 28. On the other hand, the lowest Na^+ and Ca^{2+} ion release (42 ppm and 38 ppm) was observed for 5 mol% yttrium containing glass (see Figure 9). However, the glasses containing 1 mol% and 3 mol% Y_2O_3 released 420 and 119 ppm of Na^+ ions respectively at day 28 as seen in Figure 9a. From Figure 9b, it can be seen that the Ca^{2+} ion release in-
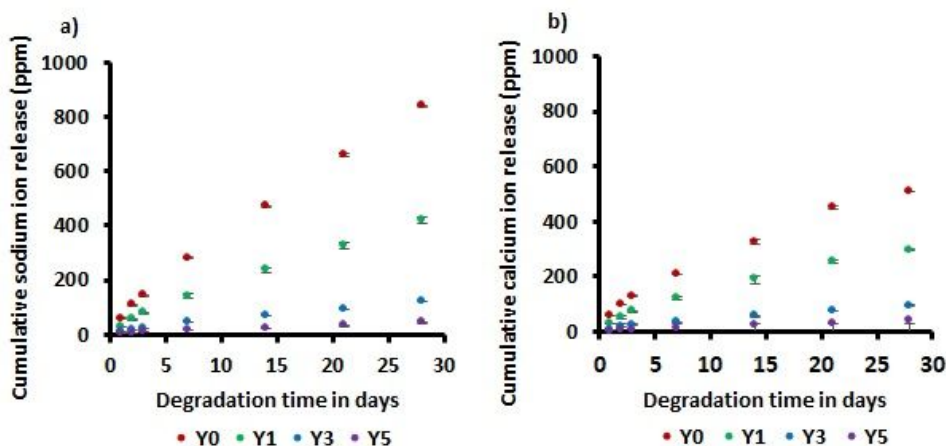

Figure 9: Cumulative ion release profile of glass discs at different glass formulation in Milli-Q water for 28 days a) Sodium ion release and b) Calcium ion release. (Error bars are also included in the data above)

creased to reach 296 ppm and 93 ppm at day 28 for Y1 and Y3 glass formulations respectively. The rates of sodium ion release were significantly greater than calcium for all glass formulations after 28 days of immersion in Milli-Q-water (see Figure 9). As expected, glasses with the highest Y_2O_3 content exhibited the lowest degree of ion release.

4 Discussion

This study investigated incorporating yttrium oxide into phosphate glasses and its effect on glass structure and chemical durability. Ternary phosphate-based glasses (PBGs) mainly consist of P_2O_5 (as network former) along with other network modifying oxides such as Na_2O and CaO. However, poor chemical durability and high solubility can limit their utility. Several authors have explored the role of yttrium oxide within silicate glass systems [33, 34, 60–63] and reported that it can act as a network former or modifier depending on the amount of Y_2O_3 present. However, detailed experimental structural analysis and physiochemical studies have not been conducted for yttrium doped phosphate-based glasses.

^{31}P NMR analysis is a valuable technique to explore the local phosphorus environment in the glass system. The NMR data obtained showed a considerable increase of Q^1 species (from 23 to 42%) with a decrease of Q^2 species (from 77 to 58%) with incorporation of 0 to 5 mol% Y_2O_3 (see Table 3). The presence of Q^1 and Q^2 species in these glasses is consistent with the work of Ahmed et al., who reported that both Q^1 (17–22%) and Q^2 (78–83%) species were identified for compositions with fixed P_2O_5 at 45 mol% [36]. Variations in Q species with addition of Y_2O_3 in the glass system were attributed to dissociation of Q^2 metaphosphate chains in effect depolymerising the phosphate network subsequently leading to an increase in Q^1 species (most likely as chain end terminators). Lee et al. conducted NMR analysis of magnesium phosphate glasses in the system of $50P_2O_5$-$5Nb_2O_5$-$(45-x)CaO$-$xMgO$ ($0 \leq \times \leq 45$ mol%) and reported that Q^1 species increased from 10 to 17% whilst Q^2 species decreased from 90 to 83% with the inclusion of MgO into the glass system [64]. In addition, they stated that the increase in Q^1 species indicated that MgO acted as a network modifier in this glass system. Moreover, as seen from Table 3, the phosphate chain length decreased from 8.69 to 4.88 with increasing Y_2O_3 content further highlighting that depolymerisation of the phosphate chains had occurred [52]. Furthermore, Table 4 showed that the O/P fraction increased from 3.11 to 3.22 with incorporation of 0 to 5 mol% Y_2O_3 in the glass system which

also indicated a high degree of depolymerisation had occurred [3]. The depolymerisation observed via increase in Q^1 species and subsequent decrease of Q^2 species, O/P ratio and the theoretical calculation of Q species suggested that yttrium acted as a network modifier in this glass system. In the NMR spectra, the chemical shifts of both Q^1 and Q^2 species moved upfield (higher negative value) with a larger change for the Q^1 species (−5.49 to −8.13 ppm) than for Q^2 (−21.74 to −21.92 ppm) as the Y_2O_3 content increased (see Table 3). Similar chemical shifts have been reported in other studies of phosphate glasses [7, 47, 65]. The decrease in chemical shift with addition of Y_2O_3 could be attributed to six fold coordinated octahedral structure of yttrium (YO_6) [40] where yttrium ions (Y^{3+}) occupy the interstitial position between PO_4 tetrahedral units forming strong cross-linking Y-O-P bonds. Cross-linking of the phosphate network would have increased with further addition of Y_2O_3. Abo-Naf et al. studied ^{27}Al NMR analysis of alumina phosphate glasses and stated that the isotropic peaks found between −16 to −22 ppm indicated octahedral structure of Aluminium (AlO_6) [66]. From ^{31}P NMR spectra, they reported that the chemical shifts of Q^1 and Q^2 species shifted from −1 to −6 ppm and −12 to −35 ppm respectively, with incorporation of 10 to 20 mol% Al_2O_3 in the glass system. This addition of network modifying alumina increased the cross-linking between phosphate tetrahedral units due to the formation of an octahedral structure of aluminium (AlO_6) [67], replacing P-O-P bonds with P-O-Al bonds. Moreover, the bonding of yttrium with BO and NBO can be explained in terms of the field strength of yttrium (~0.6 e $Å^{-2}$) which is significantly higher compared to sodium (~0.19 e $Å^{-2}$) and calcium (~0.33 e $Å^{-2}$) [14]. Higher field strength atoms lead to stronger interaction with NBOs subsequently increasing cohesion of the glass network [68], leading to formation of P-O$\cdots$Y$\cdots$O-P cross links which would have strengthened the glass network [69, 70].

From FTIR analysis, the absorption band at 703 cm^{-1} shifted to higher wavenumber with increasing Y_2O_3 content (see Figure 3) and this band was assigned to the P-O-P linkage in pyrophosphate (Q^1) group [71]. The shift of the band from 703–719 cm^{-1} was also attributed to depolymerisation of the phosphate network subsequently reducing metaphosphate chains and increasing Q^1 pyrophosphate groups. Moreover, similar behaviour was observed for the bands near 970 and 1095 cm^{-1}. Doweider et al. investigated infrared spectroscopy of lead phosphate based glasses and reported that the absorption band near ~685 cm^{-1} shifted to higher wavenumber (685–730 cm^{-1}) where modifier Pb ions entered the glass network by breaking up the P-O-P linkages creating NBOs via the formation of

Pb^{2+}-O=P ionic bonds [72]. Furthermore, the asymmetric stretching band of P-O-P (at 887 cm^{-1}) initially shifted to higher wavenumber (894 cm^{-1}) for 1 mol% Y_2O_3 and then decreased back to 893 cm^{-1} and 887 cm^{-1} for the 3 and 5 mol% yttrium oxide containing glasses, respectively. This initial increase was attributed to smaller P-O-P bond angle owing to the higher field strength of yttrium and the smaller size of the metal cations (Y^{3+}) [73]. Shih *et al.* investigated CuO containing sodium phosphate glasses and reported that the band near 900 cm^{-1} shifted to higher frequency due to higher field strength of copper ions as compared to sodium [48]. In addition, the absorption band near 900 cm^{-1} was attributed to asymmetric stretching vibration of P–O–P groups linked with linear metaphosphate chains [72, 74]. Furthermore, the band near 900 cm^{-1} shifted to lower wavenumber for 3 and 5 mol% yttrium containing PBGs which was also attributed to continuous breakdown of P-O-P chain structures due to depolymerisation of the phosphate network [72, 75]. Overall, the FTIR analysis showed good correlation with NMR and O/P ratios (as highlighted above and represented in Tables 3 and 4, respectively) [76].

Further structural investigation was conducted by heat-treating the glass samples and analysing via XRD in order to explore the crystalline phases formed at their respective crystallisation temperatures. Crystallised glass samples revealed various calcium phosphate [77] phases as shown in Figure 4. Calcium pyrophosphate ($Ca_2P_2O_7$) was predominant in the glass system along with a small amount of sodium metaphosphate ($NaPO_3$) phase. Ahmed *et al.* investigated ternary phosphate-based glasses via XRD analysis and reported that $Ca_2P_2O_7$ (calcium pyrophosphate, Q^1) phase was identified for 45 mol% P_2O_5 glasses [36]. Devi *et al.* studied TiO_2 doped phosphate-based bioactive glasses and found $NaPO_3$ (sodium metaphosphate, Q^2) phase for the glass samples they tested [8]. The Q^1 pyrophosphate species can be found in two forms, either as chain terminators or as discrete phosphate dimers. Whereas Q^2 species are long chains or rings composed of P–O–P bonds which form the backbone of the glass structure [36]. Figure 4 showed a calcium-bridged trimetaphosphate ($Na_4Ca(PO_3)_6$, *i.e.* Q^2) phase was identified for Y0 and Y1 glasses where two cyclic phosphate rings ($P_3O_9^{2-}$) are bridged by a single calcium [36, 78, 79]. Abrahams *et al.* studied alumino phosphate glasses in the $45P_2O_5$-$24CaO$-xAl_2O_3-$(31-x)Na_2O$ glass system and reported that sodium calcium metaphosphate ($Na_4Ca(PO_3)_6$) phase was identified as a major phase for 0 and 2 mol% Al_2O_3 containing glasses [80]. They suggested that this phase formed due to the Q^2 species (73–78%) being dominant within the glass for-

mulations. Moreover, the sodium yttrium pyrophosphate [$NaY(P_2O_7)$] phase had been identified for the 3 and 5 mol% Y_2O_3 containing glasses which correlated well with the reduction of Q^2 species, leading to an increase in Q^1 species. This phase consists of six-fold coordinated octahedral structure of yttrium which would increase ionic cross-linking within the phosphate network. Smith *et al.* studied alumino phosphate glasses and reported that octahedral sodium aluminium pyrophosphate ($NaAlP_2O_7$) phase was found in this glass system which had led to an increase in rigidity of the phosphate network via cross-linking [50]. Furthermore, a small amount of $NaYO_2$ phase was also identified with the incorporation of 3 and 5 mol% Y_2O_3 (see Figure 4) which was attributed to both Na^+ and Y^{3+} ions surrounded by oxygen atoms in a distorted octahedral environment due to their different ionic radii [81]. However, this phase was absent for the Y1 glass formulation which was ascribed to the low amount of yttrium content. Overall, only crystal phases containing pyro- (Q^1) and metaphosphate (Q^2) species were observed from XRD analysis which correlated well with the NMR and FTIR analyses.

From the XPS spectra, typically higher binding energy (BE) is represented by the presence of BO (P-O-P) whilst lower binding energy peak results from NBO (P-O-Y) as shown in Figure 6. The binding energy of these two peaks can be explained in terms of electronegativity and electron density. Of the elements incorporated, Y has the lowest electronegativity (1.22) [82], P has an intermediate value (2.1) [83] whilst O has the highest electronegativity (3.5) [84]. The NBO bonded with lowest electronegativity modifier atom (Y^{3+}) will subsequently increase the electron density. Thus, less energy is required to eject photoelectrons from the O 1s orbital resulting in lower binding energy for the NBO peak. On the contrary, higher energy is required for BO due to lower electron density of oxygen atoms [85]. The XPS O 1s spectra showed that inclusion of Y_2O_3 into the glass system shifted both BO and NBO peaks to higher binding energy compared to the control glass sample as represented in Figure 6. The shift in peak position to the higher binding energy could be attributed to charge differences between BO and NBO atoms with the inclusion of yttrium oxide in the glass system. Sharma *et al.* studied iron oxide doped calcium silicon phosphate glasses and reported that BO and NBO shifted to higher binding energy with the addition of 0 to 15 wt% Fe_2O_3 [86]. They stated that the shift in peak position was attributed to increasing oxidation state of the element. In addition, it was observed that the BO and NBO ratio decreased from 0.73 to 0.65 with the addition of 0 to 5 mol% Y_2O_3 in the glass system, further suggesting depolymerisation of the phos-

phate chain through breakage of P-O-P bonds [87, 88]. Furthermore, this depolymerisation effect decreased BO intensity and thereby increasing NBO intensity with increasing yttrium oxide content.

The degradation rates of the glasses investigated decreased in phosphate-buffered saline (PBS) and Milli-Q-water with increasing 0 to 5 mol% Y_2O_3 content as shown in Figure 7. As a trivalent cation (Y^{3+}) was added in place of monovalent (Na^+) cation a decrease in degradation profiles was expected [52, 89]. This decrease in degradation rate was attributed to the formation of P-O-Y bonds which were more resistant to a hydration attack than P-O-P bonds. Shi *et al.* studied chemical durability of calcium aluminophosphate glasses doped with La_2O_3 and reported that the weight loss ratio decreased from 0.71% to 0.62% with the incorporation of 2 to 2.5 mol% La_2O_3 in the glass system. They suggested that this decrease could be attributed that network modifier La_2O_3 formed more La-O-P (NBO) bonds between metal cations with phosphate glass terminal oxygen which subsequently shortened the phosphate chain due to cross-links formed in the glass structure [90]. In addition, higher field strength trivalent cations such as Y^{3+} could form stronger bonds in phosphate glass network [91–93], leading to an increase in chemical durability with increasing Y_2O_3 content. This could also be explained by the bond strength of Y-O (209 kJ/mol) being much stronger than Na-O (84 kJ/mol) [94–98]. Metwalli *et al.* investigated the structural analysis of aluminophosphate glasses and reported that higher field strength modifier cations (such as Al^{3+}) formed a rigid phosphate network which increased chemical durability due to the formation of cross-links and hydration-resistant bonds with the phosphate terminal oxygens [99]. In this study, after 28 days of immersion in degradation media, the degradation rate decreased by 29.4% in PBS and 21.3% in Milli-Q-water with the incorporation of 0 to 5 mol% Y_2O_3 content (see Figure 7). Usually, the glass dissolution process is slower in PBS compared to Milli-Q- water [38, 100] whereas in this study it was the opposite. This anomalous degradation behaviour could be attributed to the solubility effect during the degradation. It is suggested that in PBS, yttrium chloride may have formed [101] which is highly soluble in water [102]. On the contrary, yttrium hydroxide bonds can be formed in Milli Q water which is insoluble in water [103]. As a result, more dissociation in the glass network may have occurred in PBS due to high water solubility of yttrium chloride resulting in faster degradation rates in PBS.

The change in degradation was not only associated with the glass composition, concentration and rate of ions released, but also changes in pH of the surrounding medium [57] which depend on the ion exchange as well as the glass composition [100]. It is expected that glasses of higher dissolution rates would exhibit the greatest changes in pH. According to Figure 8, a slight decrease in pH was seen initially over the first 7 days for all glass formulations which then plateaued with time. No differences in pH were found for the different glass formulations. This small changes in solution pH observed were attributed to the dissociation of P-O-P bonds subsequently leading to formation of phosphoric acid in the media [36, 104].

The results of the ion release study here reflected the degradation behaviour of the Y_2O_3 containing glasses which exhibited lower ion release profiles as compared to the yttrium-free glasses (see Figure 9). Since the Y0 glass showed the highest degradation rate, it also exhibited highest level of Na^+ release which was also attributed to highest Na_2O content present in this glass formulation. Similar trend was seen for Ca^{2+} ion release profile. The decrease of Na^+ ion release observed with increasing Y_2O_3 content was ascribed to the lower amount of Na_2O compared to the control glass sample [105]. In addition, the calcium ion release rate decreased with inclusion of Y_2O_3, which was attributed to the formation of stronger ionic cross-linking bonds (Y-O-P) in the phosphate glass network. Furthermore, sodium and calcium oxide content for the Y5 glass formulation was the same (25 mol% of each). However, sodium ions were released more rapidly in comparison to the calcium for the Y5 glass which was attributed to the higher field strength and stronger cross-linking effect of Ca^{2+} as compared to Na^+ [106].

In summary, the studies above showed that yttrium oxide addition to PBGs had a significant effect on the glass structure via depolymerisation of the phosphate network. Changes in Q species with substitution of Na_2O for Y_2O_3 implied that yttrium oxide acted as a network modifier. The addition of Y_2O_3 increased the durability of the glasses which was attributed to the replacement of P-O-P bonds with hydration resistant Y-O-P bonds. It should be noted that this study was limited to incorporating up to 5 mol% Y_2O_3 content only as the glasses crystallised when further Y_2O_3 was added in this glass system [44]. Future studies will focus on manufacturing higher yttrium containing phosphate-based glasses by exploring alternate manufacturing processes. We expect that addition of 17 mol% Y_2O_3 in the phosphate glass system would decrease the degradation rate remarkably, and that we would no longer have a glass system, but instead a glass-ceramic system.

5 Conclusions

In this study, NMR analysis showed that the proportion of Q^1 species increased with the incorporation of Y_2O_3 into the glass system, leading to a subsequent decrease in Q^2 species. The BO and NBO ratio decreased with the inclusion of yttrium oxide which was been calculated from NMR and XPS analysis. The trend observed in Q^1 and Q^2 species from NMR analysis was also validated via theoretical calculations. The reduction of Q^2 species and hence BO:NBO, demonstrated that depolymerisation of phosphate network occurred with the addition of Y_2O_3 in the glass system. On the basis of NMR, XPS and FTIR analysis for this glass family series (with fixed 45 mol% P_2O_5), yttrium acted as a network modifier. Furthermore, the degradation rate decreased with the incorporation of 0 to 5 mol% Y_2O_3 content due to the formation of strong Y-O-P bonds. Therefore, varying yttrium oxide content can enable potential control over degradation and hence ion release profiles, which could be highly beneficial for radiotherapy based biomedical applications.

Ethical approval: The conducted research is not related to either human or animals use.

Conflict of Interests: The authors declare no conflict of interest regarding the publication of this paper.

References

[1] Knowles J. C., Phosphate based glasses for biomedical applications, J. Mater. Chem., 2003, 13, 2395–2401.

[2] Franks K., Salih V., Knowles J. C., Olsen I., The effect of MgO on the solubility behavior and cell proliferation in a quaternary soluble phosphate based glass system, J. Mater. Sci.: Mater. Med., 2002, 13, 549–556.

[3] Rajendran V., Devi A. V. G., Azooz M., El-Batal F. H., Physicochemical studies of phosphate based P2O5–Na2O–CaO–TiO2 glasses for biomedical applications, J. Non-Crys. Sol., 2007, 353, 77–84.

[4] Neel E. A. A., O'Dell L. A., Smith M. E., Knowles J. C., Processing, characterisation, and biocompatibility of zinc modified metaphosphate based glasses for biomedical applications, J. Mater. Sci.: Mater. Med., 2008, 19, 1669–1679.

[5] Vitale-Brovarone C., Novajra G., Milanese D., Lousteau J., Knowles J. C., Novel phosphate glasses with different amounts of TiO2 for biomedical applications: Dissolution tests and proof of concept of fibre drawing, Mater. Sci. & Eng. C, 2011, 31, 434–442.

[6] Kiani A., Hanna J. V, King S. P., Rees G. J., Smith M. E., Roohpour N., et al., Structural characterization and physical properties of P2O5–CaO–Na2O–TiO2 glasses by Fourier transform infrared, Raman and solid-state magic angle spinning nuclear magnetic resonance spectroscopies, Act. Biomater., 2012, 8, 333–340.

[7] Kiani A., Cahill L. S., Neel E. A. A., Hanna J. V, Smith M. E., Knowles J. C., Physical properties and MAS-NMR studies of titanium phosphate-based glasses, Mater. Chem. & Phy., 2010, 120, 68–74.

[8] Devi A. V. G., Rajendran V., Rajendran N., Structure, solubility and bioactivity in TiO2-doped phosphate-based bioglasses and glass–ceramics, Mater. Chem. & Phy., 2010, 124, 312–318.

[9] ElBatal F. H., Hamdy Y. M., Marzouk S. Y., UV–visible and infrared absorption spectra of transition metals-doped lead phosphate glasses and the effect of gamma irradiation, J. Non-Crys. Sol., 2009, 355, 2439–2447.

[10] Metwalli E., Karabulut M., Sidebottom D. L., Morsi M. M., Brow R. K., Properties and structure of copper ultraphosphate glasses, J. Non-Crys. Sol., 2004, 344, 128–134.

[11] Kasuga T., Abe Y., Calcium phosphate invert glasses with soda and titania, J. Non-Crys. Sol., 1999, 243, 70–74.

[12] Ahmed I., Parsons A., Jones A., Walker G., Scotchford C., Rudd C., Cytocompatibility and effect of increasing MgO content in a range of quaternary invert phosphate-based glasses, J. Biomater. App., 2010, 24, 555–575.

[13] Parsons A. J., Evans M., Rudd C. D., Scotchford C. A., Synthesis and degradation of sodium iron phosphate glasses and their in vitro cell response, J. Biomed. Mater. Res. A, 2004, 71, 283–291.

[14] Fu Y., Christie J. K., Atomic structure and dissolution properties of yttrium-containing phosphate glasses, Int. J. App. Gla. Sci., 2017, 8, 412–417.

[15] Riaz A., Lewandowski R. J., Kulik L., Salem R., Yttrium-90 radioembolization using TheraSphere® in the management of primary and secondary liver tumors, J. Nuc. Med. & Mol. Ima., 2009, 53, 311.

[16] Riaz A., Kulik L. M., Mulcahy M. F., Lewandowski R. J., Salem R., Yttrium-90 radioembolization in the management of liver malignancies, Sem. Onc., 2010, 94–101.

[17] Salem R., Hunter R. D., Yttrium-90 microspheres for the treatment of hepatocellular carcinoma: a review, Int. J. Rad. Onc.* Bio.* Phy., 2006, 66, S83–S88.

[18] Hyatt M. J., Day D.E., Glass properties in the Yttria-Alumina-Silica system, J. Am. Cer. Soc., 1987, 70, C–283.

[19] Erbe E. M., Day D. E., Chemical durability of Y2O3-Al2O3-SiO2 glasses for the in vivo delivery of beta radiation, J. Biomed. Mater. Res., 1993, 27, 1301–1308.

[20] Kawashita M., Matsui N., Li Z., Miyazaki T., Novel synthesis of yttrium phosphate microspheres for radioembolization of cancer, Mater. Sci. & Eng., 2011, 192003.

[21] Triller J., Baer H. U., Geiger L., Kinser J., Rösler H., Blumgart L. H., Radioembolisation of hepatocellular carcinoma with 90-yttrium resin particles, Eur. Rad., 1995, 5, 603–608.

[22] Burrill J., Hafeli U., Liu D. M., Advances in radioembolization-Embolics and isotopes, J. Nucl. Med. Rad. Ther., 2011, 2, 107.

[23] Burke C. W., Doyle F. H., Joplin G. F., Arnot R. N., Macerlean D. P., Fraser T. R., Cushing's disease: Treatment by pituitary implantation of radioactive gold or yttrium seeds, Int. J. Med., 1973, 42, 693–714.

[24] Taylor W. J., Corkill M. M., Rajapaske C. N., A retrospective review of yttrium-90 synovectomy in the treatment of knee arthritis., Bri. J. Rhe., 1997, 36, 1100–1105.

[25] McDevitt M. R., Chattopadhyay D., Jaggi J. S., Finn R. D., Zanzonico P. B., Villa C., et al., PET imaging of soluble yttrium-86-labeled carbon nanotubes in mice, Pl. One, 2007, 2, e907.

[26] Tickner B. J., Stasiuk G. J., Duckett S. B., Angelovski G., The use of yttrium in medical imaging and therapy: historical background and future perspectives, Chem. Soc. Rev., 2020.

[27] Salem R., Thurston K. G., Carr B. I., Goin J. E., Geschwind J. F. H., Yttrium-90 microspheres: radiation therapy for unresectable liver cancer, J. Vas. & Inter. Rad., 2002, 13, S223–S229.

[28] Borgonovo A. E., Fabbri A., Vavassori V., Censi R., Maiorana C., Multiple teeth replacement with endosseous one-piece yttrium-stabilized zirconia dental implants, Med. Oral, Pato. Oral y Cir. Buc., 2012, 17, e981.

[29] Schena E., Saccomandi P., Fong Y., Laser ablation for cancer: past, present and future, J. Func. Biomater., 2017, 8, 19.

[30] Schubert D., Dargusch R., Raitano J., Chan S. W., Cerium and yttrium oxide nanoparticles are neuroprotective, Biochem. & Biophys. Res. Comm., 2006, 342, 86–91.

[31] Cochran K. W., Doull J., Mazur M., DuBois K. P., Acute toxicity of zirconium, columbium, strontium, lanthanum, cesium, tantalum and yttrium., Arch. Ind. Hyg. & Occ. Med., 1950, 1, 637–650.

[32] DuBois K. P., Chemical toxicity of salts of lanthanum, yttrium and some other rare metals to animals, Rare Ear. Biochem. & Med. Res., 1956, 12, 91–98.

[33] Singh S., Kalia G., Singh K., Effect of intermediate oxide (Y2O3) on thermal, structural and optical properties of lithium borosilicate glasses, J. Mol. Str., 2015, 1086, 239–245.

[34] Simon V., Eniu D., Takács A., Magyari K., Neumann M., Simon S., X-ray photoemission study of yttrium contained in radiotherapy systems, J. Opto. & Adv. Mat., 2005.

[35] Fayad A. M., Abd-Allah W. M., Moustafa F. A., Effect of Gamma Irradiation on Structural and Optical Investigations of Borosilicate Glass Doped Yttrium Oxide, Silicon, 2018.

[36] Ahmed I., Lewis M., Olsen I., Knowles J. C., Phosphate glasses for tissue engineering: Part 1. Processing and characterisation of a ternary-based P2O5–CaO–Na2O glass system, Biomater., 2004, 25, 491–499.

[37] Koudelka L., Rösslerová I., Holubová J., Mošner P., Montagne L., Revel B., Structural study of PbO–MoO3–P2O5 glasses by Raman and NMR spectroscopy, J. Non-Crys. Sol., 2011, 357, 2816–2821.

[38] Brauer D. S., Rüssel C., Kraft J., Solubility of glasses in the system P2O5–CaO–MgO–Na2O–TiO2: Experimental and modeling using artificial neural networks, J. Non-Crys. Sol., 2007, 353, 263–270.

[39] Döhler F., Mandlule A., van Wüllen L., Friedrich M., Brauer D. S., 31 P NMR characterisation of phosphate fragments during dissolution of calcium sodium phosphate glasses, J. Mater. Chem. B, 2015, 3, 1125–1134.

[40] Fu Y., Christie J. K., Atomic structure and dissolution properties of yttrium-containing phosphate glasses, Int. J. App. Gla. Sci., 2017.

[41] Okura T., TANAKA M., MONMA H., YAMASHITA K., SUDOH G., New superionic conducting glass-ceramics in the system Na2O-Y2O3-Sm2O3-P2O5-SiO2: crystallization and ionic conductivity, Nip. Ser. Kyo. Gak. Ron., 2003, 111, 257–261.

[42] Nechaev G. V, Vlasova S. G., Reznitskikh O. G., Conductivity in sodium-yttrium-silicate and sodium-yttrium-phosphate glass, Gla. Phy. & Chem., 2015, 41, 64–67.

[43] SUDA S., YAMASHITA K., UMEGAKI T., Synthesis of Na+ Superionic Conductors in the Na2O-Y2O3-P2O5-SiO2 System by using metal alkoxides and Crystallization Processes from Dried Gel, Phos. Res. Bull., 1993, 3, 97–102.

[44] Arafat A., Samad S.A., Wadge M.D., Islam M.T., Lewis A.L., Barney E.R., et al., Thermal and crystallization kinetics of yttrium-doped phosphate-based glasses, Int. J. App. Gla. Sci., 2019.

[45] Zemenová P., Král R., Nitsch K., Knížek K., Cihlář A., Bystřický A., Characterization and crystallization kinetics of Er-doped Li 2 O–Y 2 O 3–P 2 O 5 glass studied by non-isothermal DSC analysis, J. Ther. Ana. & Cal., 2016, 125, 1431–1437.

[46] Martin R. A., Salmon P. S., Carroll D. L., Smith M. E., Hannon A. C., Structure and thermal properties of yttrium alumino-phosphate glasses, J. Phy.: Con. Mat., 2008, 20, 115204.

[47] Brow R. K., the structure of simple phosphate glasses, J. Non-Crys. Sol., 2000, 263, 1–28.

[48] Shih P. Y., Ding J. Y., Lee S. Y., 31P MAS-NMR and FTIR analyses on the structure of CuO-containing sodium poly-and meta-phosphate glasses, Mater. Chem. & Phy., 2003, 80, 391–396.

[49] Pickup D. M., Valappil S. P., Moss R. M., Twyman H. L., Guerry P., Smith M. E., et al., Preparation, structural characterisation and antibacterial properties of Ga-doped sol–gel phosphate-based glass, J. Mater. Sci., 2009, 44, 1858–1867.

[50] Smith J. M., King S. P., Barney E. R., Hanna J. V, Newport R. J., Pickup D. M., Structural study of Al2O3-Na2O-CaO-P2O5 bioactive glasses as a function of aluminium content, J. Chem. Phy., 2013, 138, 34501.

[51] Yung S. W., Huang Y. S., Lee Y. M., Lai Y. S., An NMR and Raman spectroscopy study of Li 2 O–SrO–Nb 2 O 5–P 2 O 5 glasses, RSC Adv., 2013, 3, 21025–21032.

[52] Hasan M. S., Ahmed I., Parsons A. J., Walker G. S., Scotchford C. A., Material characterisation and cytocompatibility assessment of quinternary phosphate glasses, J. Mater. Sci.: Mater. Med., 2012, 23, 2531–2541.

[53] Byun J. O., Kim B. H., Hong K. S., Jung H. J., Lee S., Izyneev A. A., Properties and structure of RO–Na2O–Al2O3–P2O5 (R = Mg, Ca, Sr, Ba) glasses, J. Non-Crys. Sol., 1995, 190, 288–295.

[54] Moustafa Y. M., El-Egili K., Infrared spectra of sodium phosphate glasses, J. Non-Crys. Sol., 1998, 240, 144–153.

[55] Baia L., Muresan D., Baia M., Popp J., Simon S., Structural properties of silver nanoclusters–phosphate glass composites, Vib. Spec., 2007, 43, 313–318.

[56] Ilieva D., Jivov B., Bogachev G., Petkov C., Penkov I., Dimitriev Y., Infrared and Raman spectra of Ga2O3–P2O5 glasses, J. Non-Crys. Sol., 2001, 283, 195–202.

[57] Abou Neel E. A., Chrzanowski W., Pickup D. M., O'Dell L. A., Mordan N. J., Newport R. J., et al., Structure and properties of strontium-doped phosphate-based glasses, J. Ro. Soc. Inter., 2009, 6, 435–446.

[58] Brauer D. S., Karpukhina N., Law R. V, Hill R. G., Effect of TiO2 addition on structure, solubility and crystallisation of phosphate invert glasses for biomedical applications, J. Non-Crys. Sol., 2010, 356, 2626–2633.

[59] McIntosh I. M., Nichols A. R. L., Tani K., Llewellin E. W., Accounting for the species-dependence of the 3500 cm−1 H2Ot infrared molar absorptivity coefficient: Implications for hydrated volcanic glasses, J. Ear. & Pla. Mater., 2017, 102, 1677–1689.

[60] Shakeri M. S., Rezvani M., Optical band gap and spectroscopic study of lithium alumino silicate glass containing Y3+ ions, Spec. Act. Part A: Mol. & Biomol. Spec., 2011, 79, 1920–1925.

[61] Mahdy E. A., Ibrahim S., Influence of Y2O3 on the structure and properties of calcium magnesium aluminosilicate glasses, J. Mol. Struc., 2012, 1027, 81–86.

[62] Kaur G., Kumar M., Arora A., Pandey O. P., Singh K., Influence of Y2O3 on structural and optical properties of SiO2–BaO–ZnO–xB2O3–(10- x) Y2O3 glasses and glass ceramics, J. Non-Crys. Sol., 2011, 357, 858–863.

[63] Eniu D., Simon S., Structural properties of melt versus sol-gel derived yttrium aluminosilicate systems, Ceram. Int., 2018, 44, 9581–9584.

[64] Lee S., Maeda H., Obata A., Ueda K., Narushima T., Kasuga T., Structures and dissolution behaviors of MgO–CaO–P2O5–Nb2O5 glasses, J. Non-Crys. Sol., 2016, 438, 18–25.

[65] Carta D., Knowles J. C., Smith M. E., Newport R. J., Synthesis and structural characterization of P2O5–CaO–Na2O sol–gel materials, J. Non-Crys. Sol., 2007, 353, 1141–1149.

[66] Abo-Naf S. M., Ghoneim N. A., Ei-Batal H. A., Preparation and characterization of sol–gel derived glasses in the ternary Na 2 O–Al 2 O 3–P 2 O 5 system, J. Mater. Sci.: Mater. Elec., 2004, 15, 273–282.

[67] Baskaran G. S., Mohan N. K., Rao V. V., Rao D. K., Veeraiah N., Influence of aluminium ions on physical properties of PbO-P 2 O 5-As 2 O 3 glasses, Euro. Phy. J.-App. Phy., 2006, 34, 97–106.

[68] Lin C. C., Shen P., Chang H. M., Yang Y. J., Composition dependent structure and elasticity of lithium silicate glasses: effect of ZrO2 additive and the combination of alkali silicate glasses, J. Euro. Ceram. Soc., 2006, 26, 3613–3620.

[69] Christie J. K., de Leeuw N. H., Effect of strontium inclusion on the bioactivity of phosphate-based glasses, J. Mater. Sci., 2017, 52, 9014–9022.

[70] Christie J. K., Tilocca A., Integrating biological activity into radioisotope vectors: molecular dynamics models of yttrium-doped bioactive glasses, J. Mater. Chem., 2012, 22, 12023–12031.

[71] Li Y., Weng W., Santos J. D., Lopes A. M., Structural studies of Na2O–TiO2–CaO–P2O5 system glasses investigated by FTIR and FT-Raman, Physics and Chemistry of Glasses-Euro. J. Gla. Sci. & Tech. Part B, 2008, 49, 41–45.

[72] Doweidar H., Moustafa Y. M., El-Egili K., Abbas I., Infrared spectra of Fe2O3–PbO–P2O5 glasses, Vib. Spec., 2005, 37, 91–96

[73] Lee I. H., Shin S. H., Foroutan F., Lakhkar N. J., Gong M. S., Knowles J. C., Effects of magnesium content on the physical, chemical and degradation properties in a MgO- CaO- Na2O- P2O5 glass system, J. Non-Crys. Sol., 2013, 363, 57–63.

[74] Ivascu C., Gabor A. T., Cozar O., Daraban L., Ardelean I., FT-IR, Raman and thermoluminescence investigation of P2O5–BaO–Li2O glass system, J. Mol. Struc., 2011, 993, 249–253.

[75] Rani S., Sanghi S., Agarwal A., Seth V. P., Study of optical band gap and FTIR spectroscopy of Li2O· Bi2O3· P2O5 glasses, Spec. Act. Part A: Mol. & Biomol. Spec., 2009, 74, 673–677.

[76] Chahine A., Et-Tabirou M., Pascal J. L., FTIR and Raman spectra of the Na2O–CuO–Bi2O3–P2O5 glasses, Mater. Let., 2004, 58, 2776–2780.

[77] O'Dell L. A., Neel E. A. A., Knowles J. C., Smith M. E., Identification of phases in partially crystallised Ti-, Sr-and Zn-containing sodium calcium phosphates by two-dimensional NMR, Mater. Chem. & Phy., 2009, 114, 1008–1015.

[78] Ahmed I., Lewis M. P., Nazhat S. N., Knowles J. C., Quantification of anion and cation release from a range of ternary phosphate-based glasses with fixed 45 mol% P2O5, J. Biomater. App., 2005, 20, 65–80.

[79] Ahmed I., Neel E. A. A., Valappil S. P., Nazhat S. N., Pickup D. M., Carta D., *et al.*, The structure and properties of silver-doped phosphate-based glasses, J. Mater. Sci., 2007, 42, 9827–9835

[80] Abrahams I., Franks K., Hawkes G. E., Philippou G., Knowles J., Bodart P., *et al.*, 23Na, 27Al and 31P NMR and X-ray powder diffraction study of Na/Ca/Al phosphate glasses and ceramics, J. Mater. Chem., 1997.

[81] Stagia L., Riccia P. C., Chiriua D., Napolitanob E., Enzo S., Structure Solution of NaYO2 Compound Prepared by Soft Chemistry from X-Ray Diffraction Powder Data., CHEM. ENG., 2014, 41.

[82] Ting C. C., Chang S. P., Li W. Y., Wang C. H., Enhanced performance of indium zinc oxide thin film transistor by yttrium doping, App. Sur. Sci., 2013, 284, 397–404.

[83] Serra J., González P., Liste S., Serra C., Chiussi S., León B., *et al.*, FTIR and XPS studies of bioactive silica based glasses, J. Non-Crys. Sol., 2003, 332, 20–27.

[84] Duffy J. A., Variable electronegativity of oxygen in binary oxides: possible relevance to molten fluorides, J. Chem. Phy., 1977, 67, 2930–2931.

[85] Dalby K. N., Nesbitt H. W., Zakaznova-Herzog V. P., King P. L., Resolution of bridging oxygen signals from O 1s spectra of silicate glasses using XPS: Implications for O and Si speciation, Geo. et Cosmo. Act., 2007, 71, 4297–4313.

[86] Sharma K., Deo M. N., Kothiyal G. P., Effect of iron oxide addition on structural properties of calcium silico phosphate glass/glass-ceramics, J. Non-Crys. Sol., 2012, 358, 1886–1891.

[87] Byun J. O., Kim B. H., Hong K. S., Jung H. J., Lee S. W., Izyneev A. A., Properties and structure of RONa2OAl2O3P2O5 (R = Mg, Ca, Sr, Ba) glasses, J. Non-Crys. Sol., 1995.

[88] Lucacel R.C., Ponta O., Licarete E., Radu T., Simon V., Synthesis, structure, bioactivity and biocompatibility of melt-derived P2O5-CaO-B2O3-K2O-MoO3 glasses, J. Non-Crys. Sol., 2016.

[89] Parsons A. J., Burling L. D., Scotchford C. A., Walker G. S., Rudd C. D., Properties of sodium-based ternary phosphate glasses produced from readily available phosphate salts, J. Non-Crys. Sol., 2006, 352, 5309–5317.

[90] Shi Q., Kang J., Qu Y., Liu S., Khater G. A., Li S., *et al.*, Effect of rare-earth oxides on structure and chemical resistance of calcium aluminophosphate glasses, J. Non-Crys. Sol., 2018, 491, 71–78.

[91] Du J., Molecular dynamics simulations of the structure and properties of low silica yttrium aluminosilicate glasses, J. Ame. Ceram. Soc., 2009, 92, 87–95.

[92] Shelby J. E., Introduction to glass science and technology, Roy. Soc. Chem., 2005.

[93] Uo M., Mizuno M., Kuboki Y., Makishima A., Watari F., Properties and cytotoxicity of water soluble Na2O–CaO–P2O5 glasses, Biomater., 1998, 19, 2277–2284.

[94] Dimitrov V., Komatsu T., Correlation among electronegativity, cation polarizability, optical basicity and single bond strength of simple oxides, J. Sol. Sta. Chem., 2012, 196, 574–578.

[95] Costantini A., Fresa R., Buri A., Branda F., Effect of the substitution of Y2O3 for CaO on the bioactivity of 2.5 CaO· 2SiO2 glass,

Biomater., 1997, 18, 453–458.

[96]   Vallet-Regi M., Salinas A. J., Roman J., Gil M., Effect of magnesium content on the in vitro bioactivity of CaO-MgO-SiO 2-P 2 O 5 sol-gel glasses, J. Mater. Chem., 1999, 9, 515–518.

[97]   Souza M. T., Crovace M. C., Schröder C., Eckert H., Peitl O., Zanotto E. D., Effect of magnesium ion incorporation on the thermal stability, dissolution behavior and bioactivity in Bioglass-derived glasses, J. Non-Crys. Sol., 2013, 382, 57–65.

[98]   Ma J., Chen C. Z., Wang D. G., Hu J. H., Effect of magnesia on structure, degradability and in vitro bioactivity of CaO−MgO−P2O5−SiO2 system ceramics, Mater. Let., 2011, 65, 130–133.

[99]   Metwalli E., Brow R. K., Modifier effects on the properties and structures of aluminophosphate glasses, J. Non-Crys. Sol., 2001, 289, 113–122.

[100] Cozien-Cazuc S., Parsons A. J., Walker G. S., Jones I. A., Rudd C. D., Real-time dissolution of P40Na20Ca16Mg24 phosphate glass fibers, J. Non-Crys. Sol., 2009, 355, 2514–2521.

[101] Huang L., Qiao D., Green B. A., Liaw P. K., Wang J., Pang S., *et al.*, Bio-corrosion study on zirconium-based bulk-metallic glasses, Intermet., 2009, 17, 195–199.

[102] Crew M. C., Steinert H. E., Hopkins B. S., The solubility of Yttrium salts, J. Phy. Chem., 2002, 29, 34–38.

[103] Malik J., Tilocca A., Hydration effects on the structural and vibrational properties of yttrium aluminosilicate glasses for in situ radiotherapy, J. Phy. Chem. B, 2013, 117, 14518–14528.

[104] Ahmed I., Cronin P. S., Abou Neel E. A., Parsons A. J., Knowles J. C., Rudd C. D., Retention of mechanical properties and cytocompatibility of a phosphate-based glass fiber/polylactic acid composite, J. Biomed. Mater. Res. Part B: App. Biomater., 2009, 89, 18–27.

[105] Neel E. A. A., Ahmed I., Blaker J. J., Bismarck A., Boccaccini A. R., Lewis M. P., *et al.*, Effect of iron on the surface, degradation and ion release properties of phosphate-based glass fibres, Act. Biomater., 2005, 1, 553–563.

[106] Felfel R. M., Ahmed I., Parsons A. J., Palmer G., Sottile V., Rudd C. D., Cytocompatibility, degradation, mechanical property retention and ion release profiles for phosphate glass fibre reinforced composite rods, Mater. Sci. & Eng. C, 2013, 33, 1914–1924.

[107] Sene F. F., Martinelli J. R., Gomes L., Synthesis and characterization of niobium phosphate glasses containing barium and potassium, J. Non-Crys. Sol., 2004, 348, 30–37.

[108] Foroutan F., De Leeuw N. H., Martin R. A., Palmer G., Owens G. J., Kim H. W., *et al.*, Novel sol–gel preparation of (P 2 O 5) 0.4–(CaO) 0.25–(Na 2 O) X–(TiO 2)(0.35- X) bioresorbable glasses (X= 0.05, 0.1, and 0.15), J. Sol-Gel Sci. & Tech., 2015, 73, 434–442.

[109] Ciceo-Lucacel R., Radu T., Ponta O., Simon V., Novel selenium containing boro-phosphate glasses: Preparation and structural study, Mater. Sci. & Eng. C, 2014, 39, 61–66.

[110] Lu M., Wang F., Liao Q., Chen K., Qin J., Pan S., FTIR spectra and thermal properties of TiO2-doped iron phosphate glasses, J. Mol. Struc., 2015, 1081, 187–192.